

# Wearable nanoplasmonic sensor based on surface-enhanced Raman scattering for multiplexed analysis of sweat

NAN WANG,<sup>1,†</sup> YOU LIANG WENG,<sup>2,†</sup> YI LIU,<sup>1</sup> YANGMIN WU,<sup>1</sup> SHUOHONG WENG,<sup>1</sup> YI SHEN,<sup>1,4</sup> SHANGYUAN FENG,<sup>1,3,5</sup> AND DUO LIN<sup>1,\*</sup> 

<sup>1</sup>Key Laboratory of OptoElectronic Science and Technology for Medicine, Ministry of Education, Fujian Provincial Key Laboratory for Photonics Technology, Fujian Normal University, Fuzhou 350117, China

<sup>2</sup>Department of Radiation Oncology, Clinical Oncology School of Fujian Medical University, Fujian Cancer Hospital, Fuzhou 350014, China

<sup>3</sup>Fujian Provincial Key Laboratory for Advanced Micro-nano Photonics Technology and Devices, Institute for Photonics Technology, Quanzhou Normal University, Quanzhou 362000, China

<sup>4</sup>e-mail: yishen@fjnu.edu.cn

<sup>5</sup>e-mail: syfeng@fjnu.edu.cn

<sup>†</sup>These authors contributed equally to this work.

\*Corresponding author: duo@fjnu.edu.cn

Received 10 March 2025; revised 15 May 2025; accepted 25 May 2025; posted 27 May 2025 (Doc. ID 561426); published 1 August 2025

Wearable sweat sensors that enable non-invasive sampling, efficient and rapid detection, and real-time monitoring capabilities have become an integral and critical component of human health management, with the potential to provide meaningful clinical information related to physiologic diseases in the healthcare field. Here, a flexible nanoplasmonic paper-based sensor based on surface-enhanced Raman scattering (SERS) was developed, in which silver nanoparticles were loaded in the cellulose paper to enhance the Raman signals of targets via the generation of SERS “hotspots.” By incorporating the filter paper channel with a natural core absorbing liquid, the multi-functional chip is formed, which integrates the collection, transmission, and detection of trace sweat. This paper-based chip is soft and stretchable, and fits perfectly onto the human skin surface without causing any damage or irritation. Combined with a hand-held Raman spectrometer, quantitative detection of multiple sweat components can be achieved with the limit of detection of 17 and 1  $\mu\text{mol/L}$  for uric acid and glucose, respectively, and the measurable range is 4–7.5 for pH, enabling wearable and *in-situ* optical sensing for sweat markers under the condition of human physiology and pathology, within only 5 min for uric acid and glucose detection. This wearable biosensor would provide, to our knowledge, a new way for continuously monitoring the health status by collection and analysis of multiple components in human sweat, contributing to point-of-care testing and personalized medicine applications. © 2025 Chinese Laser Press

<https://doi.org/10.1364/PRJ.561426>

## 1. INTRODUCTION

The advancement in flexible electronics has significantly bolstered the evolution of wearable sensors, facilitating their transition from theoretical research to practical implementation. Wearable biosensors, designed with biosensor components integrated onto flexible substrates, possess intrinsic qualities of flexibility, lightness, and stretchability. These attributes enable seamless adherence to skin or clothing surfaces, bridging the gap between traditional rigid silicon-based sensors and supple biological systems. Consequently, they facilitate continuous, real-time non-invasive monitoring of human physiological parameters, offering users convenient, dynamic, and personalized access to health data [1–3]. One of the important applications of wearable biosensors is to monitor biological fluids,

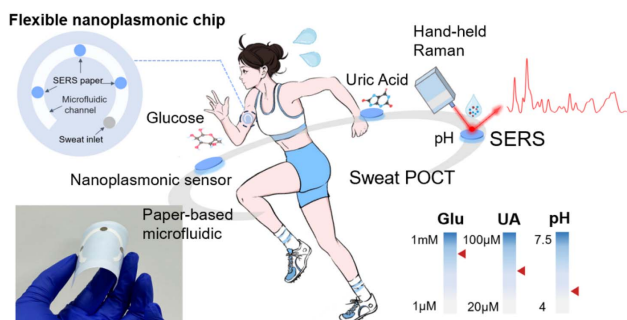
such as sweat [4–6], tears [7,8], saliva [9,10], and tissue fluids [11,12], which carry complex biomolecular signatures of the human body and have piqued researchers’ interest owing to their easy accessibility for sampling. Among these, sweat stands out for its richness in metabolites and electrolytes like glucose, lactate, and uric acid, providing detailed physiological insights at the molecular level. For instance, as the end product of purine metabolism, the elevated level of uric acid not only directly leads to gout (an inflammatory arthritis suffered by millions of people worldwide), but in severe cases, it is also a precursor to cardiovascular diseases and renal dysfunction [13–16]. Similarly, prolonged high blood glucose levels lead to diabetes, triggering a spectrum of complications including neuropathy and retinopathy [17,18]. Studies indicate a robust

correlation between blood glucose levels and sweat composition, suggesting the potential for monitoring glucose levels through sweat analysis, sidestepping the discomfort of traditional blood-based glucose monitoring methods [19]. The pH value of sweat, as a dynamic indicator reflecting the acid-base balance of blood, can not only assess the intensity of exercise and dehydration status in real time, but also indicate metabolic abnormalities such as cystic fibrosis [20–22]. Wearable sweat sensors excel at detecting biomarkers and disease markers at the molecular level within sweat, ensuring immediate, continuous, non-intrusive, and precise analysis, thereby reflecting the body's physiological and pathological state [23]. Presently, wearable sweat sensors predominantly rely on electrochemical and colorimetric methodologies. Electrochemical-based sensors allow for detecting various sweat chemicals, including electrolytes, metabolites, and hormones, by translating biochemical data into readable electrical signals on specialized electrode surfaces, conveying the analyte concentration [14,24–28]. Conversely, optical sensors leveraging colorimetric or fluorescent techniques boast ease of integration into wearables due to their streamlined preparation process, lightweight profile, and autonomy from external power sources [29–31]. These sensors function based on chemical reactions between the analyte and color developers, manifesting visible alterations under light stimulation, thereby facilitating qualitative or semi-quantitative assessments via naked-eye inspection or visual readout devices [23]. However, electrochemical sensors are sensitive to environmental factors, such as temperature and humidity, leading to fluctuations in sensor stability and accuracy. In addition, such sensors necessitate high-quality working electrodes and intricate circuit designs, thereby augmenting the complexity and expense of the device. Furthermore, they exhibit constrained anti-interference capabilities. The signals emitted by these sensors typically rely on substantial electrochemical analysis equipment for acquisition and processing, which hinders the miniaturization and portability of the entire system [32]. On the other hand, colorimetric and fluorescence techniques are highly susceptible to variations in light and color, rendering them prone to subjective judgment errors. The naked eye often struggles to discern subtle color changes among samples, necessitating detection under specific conditions to procure accurate results. Consequently, this poses limitations on the capacity for long-term continuous monitoring with such sensors [28]. Therefore, the development of novel sensing technologies to enhance sweat analysis assumes paramount importance.

Surface-enhanced Raman scattering (SERS) based on localized surface plasmon resonance (LSPR) is a spectroscopic analysis technique that not only inherits from spontaneous Raman characteristics like “biomolecular fingerprint” analytical nature, but also enables the ultra-sensitive examination with even single-molecule level. Compared with traditional optical detection methods, SERS has many advantages. For example, the SERS signals of water are extremely weak, making it more suitable for the detection of biological samples with high water content as compared with absorption spectroscopy. In addition, the bandwidth of SERS peaks is usually 10–100 times narrower than that of fluorescence spectra, allowing multiplex detection under single wavelength excitation. Moreover, it is regarded as an ideal tool for long-term biological monitoring due to its ability to resist

photobleaching and photodegradation. These advantages make SERS technology an effective analysis tool for studying complex biological systems [33–36]. Owing to the above-mentioned advantages, SERS has been widely used in the biomedical field ranging from protein, nucleic acid, and cells to body fluid and tissue [37,38]. Although traditional rigid SERS substrates (such as precious metal nanostructures supported on silicon wafers or glass) have a high signal enhancement factor and good stability, they have problems such as poor mechanical flexibility and low adhesion to curved surfaces, which limit their application in wearable detection [39–41]. In contrast, flexible SERS substrates have significant advantages: excellent stretchability and adhesion enable them to closely adhere to the skin surface, ensuring detection stability; good breathability and biocompatibility make it suitable for long-term wearing. Meanwhile, it is easy to integrate with flexible electronics, providing a new solution for real-time and dynamic monitoring [42–45]. Recently, wearable sweat sensors based on flexible SERS substrates have attracted much attention. For example, Chen *et al.* combined SERS technology with image recognition technology to design a wearable sensor that can sensitively detect uric acid in sweat and obtain the volume and pH value of sweat via a smartphone photo [46]. Wang *et al.* developed a flexible SERS wearable sensor based on cellulose nanocomposite hydrogel [32]. The network structure of the hydrogel can retain small molecules and adsorb sweat through hydrophilic groups, which enables effective collection and quantitative analysis of urea and uric acid in sweat by diffusing sweat into the hydrogel. Notably, the qualitative detection of sweat sensors can only determine whether there is a certain component in sweat, and there are certain limitations in the use scenario, so the accuracy of qualitative detection is far from sufficient for sweat sensors [47]. Compared with the single component detection of sweat [46,48], the multi-component detection of sweat can provide data of multiple physiological indicators at the same time, and reflect the physiological state of the human body from multiple angles, which improves the detection efficiency. It is worth noting that if various components of sweat were adopted in the non-labeled SERS detection method, there would often be problems such as similar or even overlapping detection of molecular characteristic peaks, resulting in reduced differentiation of multiple detected substances [49]. With the development of Raman spectroscopy instruments in the direction of miniaturization, SERS technology has gradually gotten away from the dependence on large-scale Raman instruments, which is crucial for realizing real-time detection, on-site analysis, and continuous monitoring. However, some wearable devices still need to rely on traditional large-scale Raman instruments for detection, which has certain limitations in terms of application scenarios and portability [32]. In addition, there are no reports of wearable sweat sensors using hand-held Raman instruments to achieve accurate quantitative detection of multiple trace components of human sweat uric acid, glucose, and pH, which is particularly important for achieving *in-situ* detection of sweat, better reflecting the physiological state and health status of the human body, or for early screening of diseases.

In this study, we designed a wearable sensor based on a flexible SERS substrate, which combines a paper microfluidic system and can directly capture and transfer sweat in a state of motion or



**Scheme 1.** Schematic diagram of wearable nanoplasmonic sweat sensor based on flexible SERS substrate.

low sweat secretion, and provide rapid, accurate, and noninvasive quantitative analysis of human sweat via nanoplasmonic sensors (Scheme 1). Highly sensitive SERS quantitative analysis of uric acid, glucose, and pH in sweat was achieved by utilizing the high enhancement benefits of silver nanoparticles (AgNPs) and the natural 3D hotspot structure of a cellulose paper base. The wearable device is soft, flexible, and stretchable, and can be attached to human skin without causing chemical or physical irritation. In addition, the design uses a hand-held Raman spectrometer to acquire signals, which overcomes the limitations of large Raman instruments in use scenarios and allows for immediate detection, continuous monitoring, and on-site analysis.

## 2. MATERIALS AND METHODS

### A. Experimental Materials

Hydroxylamine hydrochloride ( $\text{NH}_3\text{OHCl}$ ), sodium hydroxide ( $\text{NaOH}$ ), silver nitrate ( $\text{AgNO}_3$ ), rhodamine 6G (R6G), 4-mercaptobenzoic acid (4-MBA), 4-mercaptobenzeneboronic acid (4-MPBA), uric acid, glucose, fructose, galactose, and sucrose were purchased from Aladdin Reagent (Shanghai) Co., Ltd; cellulose chromatography paper (Whatman No. 1 grade) was obtained from Fisher Scientific; cellulose qualitative and quantitative filter paper was purchased from Nantong Hai Rui Experimental Equipment Co. Artificial sweat was purchased from Shanghai Yuanye Biotechnology Co. Medical double-sided adhesive tape was purchased from 3M Company. Double-sided carbon tape was purchased from Shenzhen Nader Adhesive Technology Co. Medical waterproof PU film was purchased from Corfu Medical Equipment Co. Ultrapure water was purchased from Milli-Q (resistivity  $18.2 \text{ M}\Omega \cdot \text{cm}$ ). All drugs were used directly without further purification.

### B. Experimental Apparatus

Scanning electron microscopy (SEM) images of AgNPs were obtained using a scanning electron microscope (Gemini 300, ZEISS, Germany). Transmission electron microscopy (TEM) images were obtained using a transmission electron microscope (JEM F200, JEOL, Japan). Absorption spectra of AgNPs were obtained using an absorption spectrometer (Lambda 950, PerkinElmer, USA). SERS spectra were acquired using a hand-held Raman spectrometer (RMS2000, Shanghai Oceanhood Optoelectronics Technology Co., Ltd., China), using an excitation wavelength of 785 nm, a laser power of 10 mW, and an integration time of 5 s. In order to ensure the reliability of Raman spectra,

five points were randomly collected for each sample and the average spectrum was calculated. To conduct real sweat measurement, following the use of alcohol to rub the forearm of the volunteer for cleansing purposes, the wearable device was securely attached to the same forearm. Subsequently, after allowing the volunteer to engage in exercise for 30 min, the SERS spectrum was collected.

### C. Synthesis of AgNPs

AgNPs were prepared by reduction of hydroxylamine hydrochloride as proposed in the study of Leopold and Lendl [50]. Briefly, 4.5 mL of  $\text{NaOH}$  solution (0.1 M,  $1 \text{ M} = 1 \text{ mol/L}$ ) was added to 5 mL of hydroxylamine hydrochloride solution ( $6 \times 10^{-2} \text{ M}$ ), the mixture was quickly added to 90 mL of  $\text{AgNO}_3$  solution ( $1.1 \times 10^{-3} \text{ M}$ ), and the AgNPs were obtained by shaking uniformly using a magnetic stirrer until the solution took on a milky gray color. Finally, the AgNPs were stored in a refrigerator at  $4^\circ\text{C}$ , protected from light, and stored for backup. Unmodified negatively charged AgNPs were used as the enhancement substrate for SERS detection. The surface-modified 4-MBA AgNPs were obtained by mixing  $10^{-3} \text{ M}$  4-MBA with AgNPs and sonicated for 30 min.

### D. Preparation of Flexible Substrate

The cellulose paper was prepared into a circle with a diameter of 5 mm, the pre-prepared AgNPs were centrifuged at 8000 r/min for 10 min, the desired concentration of AgNPs was prepared by removing the supernatant, and a certain amount of concentrated AgNPs were added dropwise to each paper substrate in order to make the AgNPs adsorbed uniformly on the surface of the paper, which was dried naturally at room temperature to obtain the AgNPs paper substrate. The double-sided carbon tape, pre-cut shaped paper microfluidic channels, and AgNPs paper were sequentially assembled on medical double-sided adhesive tape, and finally encapsulated with a transparent and thin medical waterproof PU film.

## 3. RESULTS AND DISCUSSION

### A. Design and Characterization of the Wearable Nanoplasmonic Paper-Based Sweat Analysis Chip

Figure 1(a) shows a conceptual diagram of a wearable sweat sensor that combines flexible SERS substrate technology and microfluidic technology. The device can be lightly fitted to the human arm. After pressure is applied via the sweat glands, the collection and transport of trace amounts of sweat over the microfluidic channel are achieved through the capillary action of the cellulose paper substrate and the ability of the natural core to absorb liquids, which results in the *in-situ* collection and transfer of the sweat analyte on a nanoplasmonic sensor for SERS detection. Figures 1(a) and 1(b) show the stacked functional layer view and top view, respectively, of the sensor, which is designed to consist of five main components (from bottom to top). (i) Double-sided adhesive layer: a stretchable medical double-sided adhesive with a sweat inlet (6 mm) of the same size as the microfluidic sweat channel. It is biocompatible and sterile, maximizing sweat collection while forming a strong interface between the paper microfluidic layer and the skin without causing skin irritation. (ii) Laser blocking layer: a carbon black tape, matching the dimensions of the nanoplasmonic sensor, functions as a laser-blocking layer. This layer is implemented to prevent laser energy

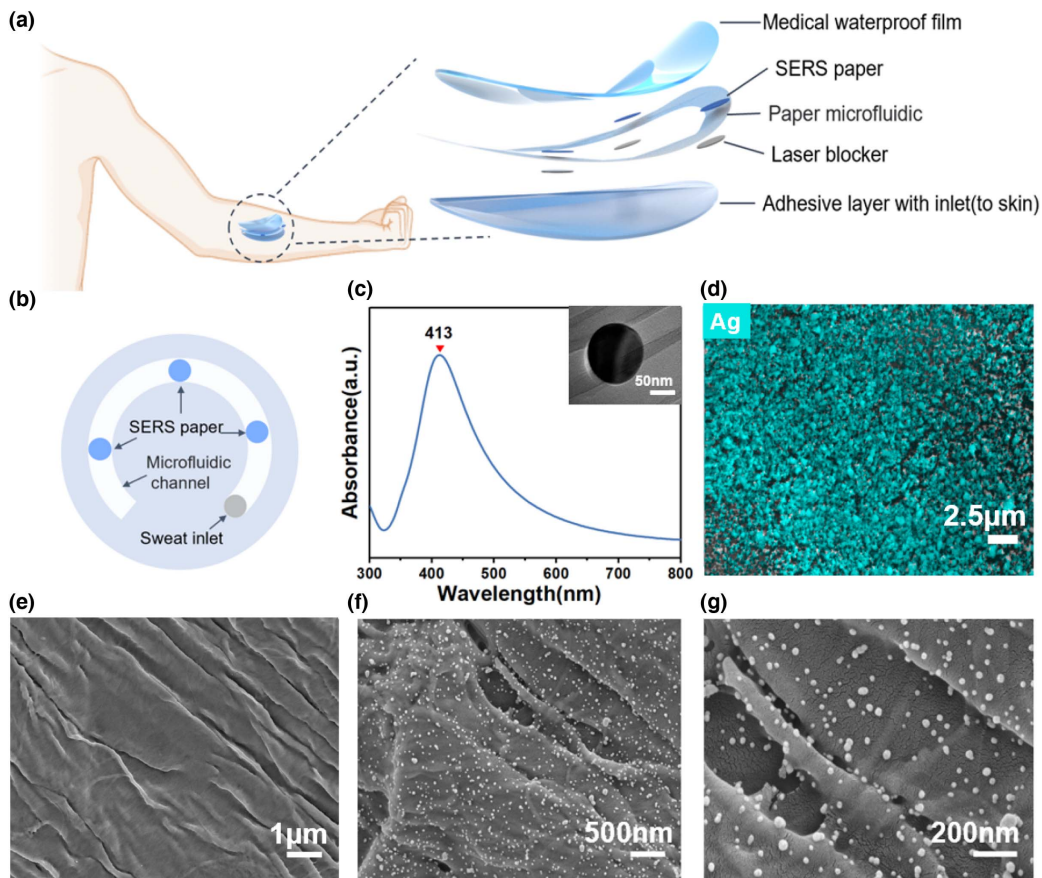


**Fig. 1.** Wearable nanoplasmonic paper-based sweat analysis chip. (a) Schematic of the functional layer stacking of the wearable nanoplasmonic paper-based sweat analysis chip. (b) Top view schematic of the wearable nanoplasmonic paper microfluidic chip. (c) UV-visible-absorption spectra of AgNPs, and the inset is a TEM image of AgNPs. (d) Elemental analysis map of the nanoplasmonic SERS sensor. (e) SEM image of cellulose paper without any modification. (f) SEM image of AgNPs massively distributed in the 3D structure of cellulose paper. (g) SEM image of AgNPs attached to cellulose paper.

exposure to human skin during *in-situ* SERS detection, thereby mitigating the risk of skin damage. (iii) Cellulose paper microfluidic layer: the sweat microfluidic channel composed of cellulose paper with a certain width (6 mm) does not require additional pumps or pressures, and can easily realize the capture and transportation of biofluids through its own capillary action. The paper microfluidic channel is soft, flexible, and malleable, inexpensive and easy to obtain, and simple and easy to use. (iv) Nanoplasmonic sensor layer: the nanoplasmonic sensor consists of AgNPs-loaded paper with high SERS benefits adsorbed on the surface, referred to as AgNPs paper in the following discussion. The SERS signal is enhanced by the localized electromagnetic enhancement effect, especially in the narrow gaps of some nanoplasmonic structures, where a strong localized electromagnetic field enhancement is produced by the concentration of light, known as the “hotspot” effect [51,52]. The 3D hierarchical fiber structure of cellulose paper provides a large number of sites for the attachment of AgNPs, resulting in an abundant hotspot effect, which is the key to obtaining strong SERS signals. On the other hand, cellulose paper has a low background signal and it also has the ability to absorb liquids, which enables simultaneous concentration of target molecules during SERS measurements [53]. Trace amounts of sweat produced by sweat glands are captured by AgNPs paper immobilized in the sweat channel

via paper microfluidics, thus enabling SERS detection of sweat analytes. (v) Top encapsulation layer: the transparent and thin medical PU film is used to encapsulate the whole device to prevent contamination from the environment. The top encapsulation layer is breathable, waterproof, and antimicrobial, and the material is soft and comfortable for long time wearing. Meanwhile the transparent material can be used to perform *in-situ* SERS detection better.

The enhancement of the SERS signal depends to a large extent on the interaction between the adsorbed molecules and the surface of the nanoplasmonic nanostructures. Typically, the classical SERS substrates are gold (Au), silver (Ag), or copper (Cu). Gold and silver are more commonly used as SERS substrates because they have a better enhancement effect and are more stable in air compared to copper [54]. As compared with AuNPs, silver nanostructures are not only more cost-effective but also produce higher SERS signal enhancement [55]; we thus chose filter paper loaded with AgNPs with high enhancement benefits as the SERS substrate. The UV-visible-absorption spectra of AgNPs [Fig. 1(c)] showed that the maximal peak of AgNPs is at 413 nm, and from the TEM interpolation in Fig. 1(c), it can be seen that the synthesized AgNPs are rounded in shape and have a size of about 80 nm. According to the elemental analysis plot of Fig. 1(d), it can be seen that a large number of AgNPs are

uniformly attached to the cellulose filter paper, which is essential for obtaining a uniform Raman signal on the SERS substrate. On the other hand, as shown in the SEM images of the untreated bare paper in Fig. 1(e), it can be seen that the inherent folded structure of the cellulose paper provides abundant attachment sites. Subsequently, AgNPs are massively distributed within the 3D structure of the cellulose paper, and lead to the occurrence of a strong hot-spot effect in the narrow gaps of various plasmas, substantially improving the sensitivity of the SERS signal [Figs. 1(f) and 1(g)].

## B. Optimization and Performance Exploration of Nanoplasmonic Sensors

The nanoplasmonic sensor is the core component of the wearable nanoplasmonic paper sweat analysis chip, which is responsible for generating highly sensitive SERS signals and plays an important role in the quantitative analysis of the detectors. To ensure the reliability of the experimental results, we have optimized the conditions and studied the performance of the nanoplasmonic sensor. AgNPs were prepared according to the method of rapid reduction of silver nitrate with hydroxylamine hydrochloride at room temperature proposed in the study of Leopold and Lendl [50], and the prepared AgNPs were attached to cellulose filter paper with a 3D hierarchical

structure to obtain a SERS substrate with abundant hotspots. In order to explore the optimal conditions for nanoplasmonic sensors, we explored in advance the best measuring distance and angle when performing the SERS via the hand-held Raman spectrometer, and we tested the SERS spectra of rhodamine 6G (R6G) deposited AgNPs on filter papers with different apertures. Since the size of the formulated AgNPs was fixed (60–80 nm), by changing the aperture of the nanoparticle attachment platform, the plasma attachment state as well as the hotspot gap could be adjusted to obtain the SERS enhancement with differentiation. Too small aperture of the filter paper will affect the liquid flow rate, and surface tension and capillarity prevent the liquid from freely passing through the aperture, which may result in the liquid not being able to fully penetrate into the filter paper and exhibit hydrophobic-like characteristics, which has an impact on both the intensity and homogeneity of the SERS signal. The excessive enlargement of apertures can diminish the effective trapping capacity of filter paper for plasmonic nanoparticles, impacting the reliability of SERS enhancement. In this study, we evaluated the characteristic peaks of the R6G molecule at 763, 1174, and 1353  $\text{cm}^{-1}$ , corresponding to the C-H bond bending vibration, the oxidation vibration on the benzene ring, and the C-C bond vibration of R6G. The results in Figs. 2(b) and 2(c) illustrate

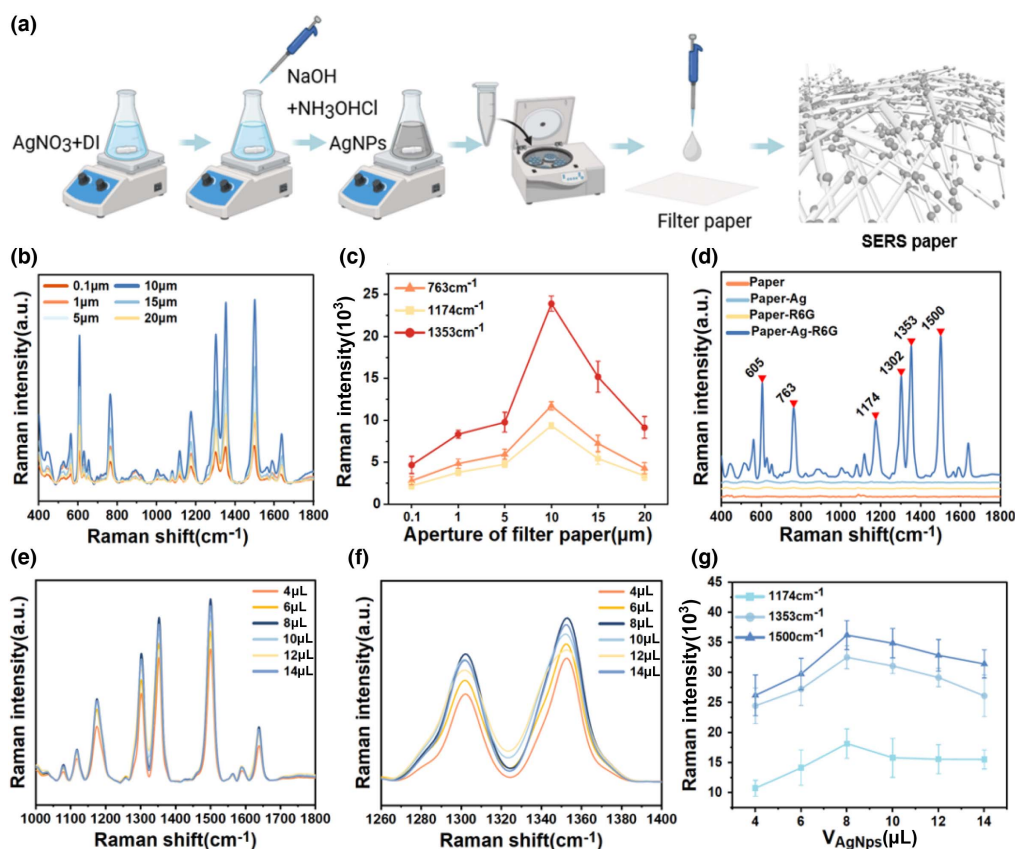


**Fig. 2.** Optimization of conditions for nanoplasmonic sensors. (a) Preparation process of nanoplasmonic sensor. (b) SERS spectra of R6G ( $10^{-3}$  M) in the nanoplasmonic sensor with different apertures. (c) SERS signal intensity of R6G characteristic peaks in different apertures of the nanoplasmonic sensor. (d) Raman spectra of R6G on different substrates. (e) SERS spectra of R6G in nanoplasmonic sensors with dropwise addition of different volumes of AgNPs. (f) Magnified view of the SERS spectra of R6G on nanoplasmonic sensor with dropwise addition of different volumes of AgNPs at 1260–1400  $\text{cm}^{-1}$ . (g) SERS signal intensity of the characteristic peak of R6G in the nanoplasmonic sensor with different volumes of AgNPs added dropwise.

that the signal intensity of R6G initially rises and then declines with increasing filter paper aperture. Consequently, a filter paper with a 10  $\mu\text{m}$  aperture was chosen as the optimal support platform for subsequent experiments. To assess the SERS enhancement effect of AgNPs, we measured Raman spectra of R6G on the paper sensing platform with and without AgNPs [Fig. 2(d)]. Notably, the background signal from the cellulose filter paper is minimal and does not interfere with the target analytes. Additionally, the Raman signals of R6G are faint on bare paper, while the weak signals can be dramatically enhanced using paper loaded with AgNPs. The prominent enhancement of the typical Raman peaks of R6G suggests a substantial SERS enhancement effect conferred by the fabricated nanoplasmonic sensor. Further refining the preparation conditions of the nanoplasmonic sensors, we fabricated sensors with varying volumes of AgNPs on filter paper of the same size to compare their SERS enhancement effect on R6G [Figs. 2(e)–2(g)]. Notably, minimal addition of AgNPs results in weak hotspot generation due to large nanoparticle spacing, yielding a diminished SERS signal. Conversely, an excessive volume of AgNPs leads to agglomeration and the formation of larger clusters, complicating the distribution of the local electric field and affecting the SERS enhancement effect. These findings, as shown in Fig. 2(g), underscore this phenomenon. Incremental addition of AgNPs yielded an initial increase and subsequent decrease in the SERS signal intensity of R6G, leading us to select the nanoplasmonic sensor with 8  $\mu\text{L}$  volume of AgNPs for further experiments.

Following the establishment of optimal experimental conditions for sensor preparation, the performance of the sensor was investigated by employing R6G molecules as a model. Raman spectra of R6G solutions across various concentrations

( $10^{-3}$ – $10^{-9}$  M) were acquired using a hand-held Raman spectrometer, as depicted in Fig. 3(a). Even at a concentration as low as  $10^{-9}$  M, distinctive characteristic peaks of R6G remained evident, revealing the exceptional sensitivity of this SERS sensor. Ensuring uniformity and stability in test results is a crucial aspect for paper-based sensors when conducting assays at low concentrations. As demonstrated in Figs. 3(b) and 3(c), SERS spectra obtained from 30 randomly selected points on the AgNPs paper exhibited consistently intense characteristic peaks. The Raman signal intensities from the  $1353\text{ cm}^{-1}$  peak representing the C–C vibration on the R6G benzene ring displayed a low relative standard deviation (RSD) of 5.36%, highlighting the homogeneity of SERS signals from the nanoplasmonic paper sensor. Subsequently, average spectra of R6G from five distinct batches of AgNPs-loaded paper exhibited remarkable consistency and reproducibility, as illustrated in Fig. 3(d) with RSD of 3.69%. To assess the temporal stability of the sensor, long time tests were conducted on the same batch of AgNPs paper every 7 days [Figs. 3(e) and 3(f)]. The acquired SERS signals remained relatively stable over different time intervals and retained excellent SERS performance even after 30 days. Nonetheless, a slight decrease in SERS signals (27%) was observed over time, attributed to the oxidation or aggregation of the surface AgNPs. These findings underscore the sensor's impressive sensitivity, uniformity, reproducibility, and its ability to sustain continuous stability and SERS activity over an extended duration.

### C. SERS Sensor for Detection of Uric Acid in Sweat

The label-free SERS technique was employed to sensitively detect uric acid in sweat, as illustrated in Fig. 4(a), facilitating rapid analysis of trace sweat without the need for additional markers and streamlining the experimental procedure. SERS spectra of

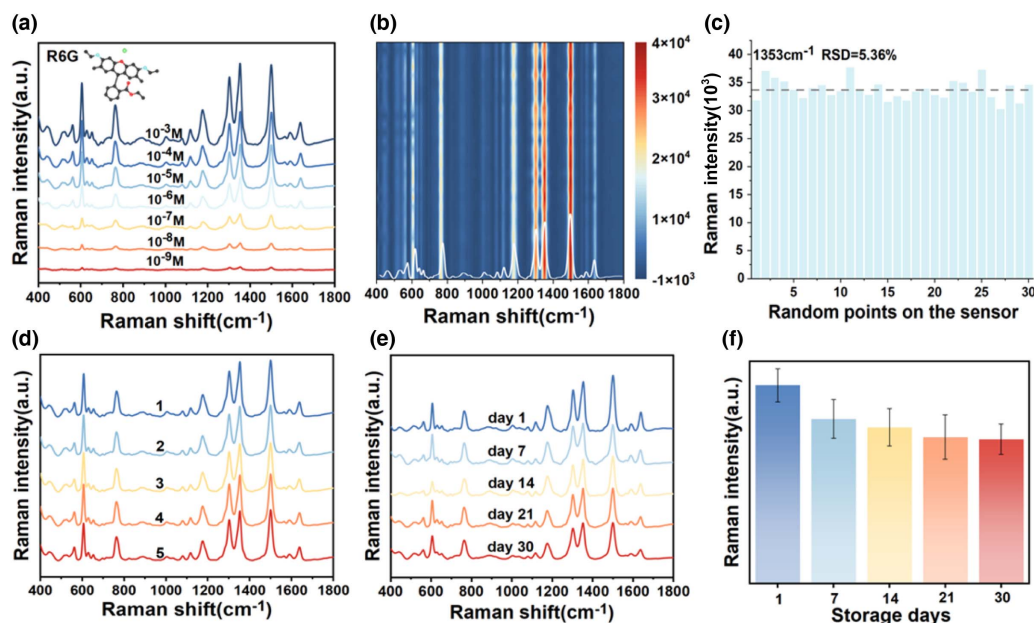


**Fig. 3.** Performance exploration of the nanoplasmonic sensor. (a) SERS spectra of different concentrations ( $10^{-3}$ – $10^{-9}$  M) of R6G on the nanoplasmonic sensor. (b) SERS spectra of 100 bars of R6G ( $10^{-3}$  M) obtained from random locations on the nanoplasmonic sensor. (c) SERS intensities of 30 random points on the nanoplasmonic sensor at the characteristic peak of R6G at  $1353\text{ cm}^{-1}$ . (d) SERS spectra of R6G from different batches of the nanoplasmonic sensor. (e) SERS spectra of R6G for nanoplasmonic sensors from the same batch at different times. (f) Signal stability of the nanoplasmonic SERS sensor over time.

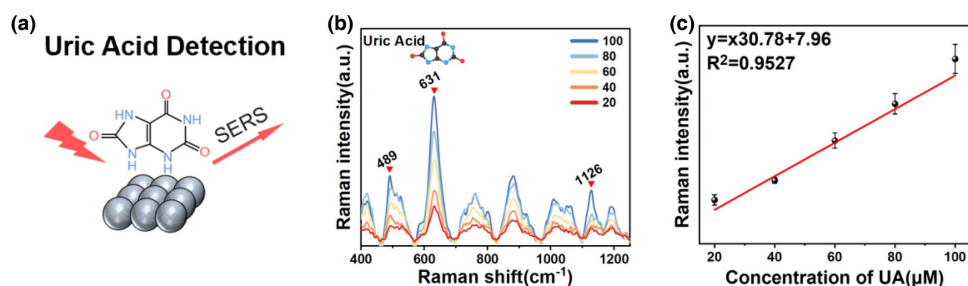


**Fig. 4.** SERS sensor for detecting uric acid in sweat. (a) Schematic diagram of the non-labeled approach to detect uric acid. (b) SERS spectra of different concentrations of uric acid (20–100  $\mu\text{M}$ ) in sweat. (c) Linear fitting curve of the SERS intensity of uric acid at the characteristic peak  $631\text{ cm}^{-1}$ .

uric acid in sweat with concentrations from 20 to 100  $\mu\text{M}$  are displayed in Fig. 4(b), encompassing the physiological and pathological concentration ranges of uric acid found in the sweat of both healthy individuals and patients with conditions such as gout and hyperuricemia [48,56]. A linear fitting curve was generated based on the characteristic peak at  $631\text{ cm}^{-1}$  associated with the deformation of the skeleton ring of uric acid, depicted in Fig. 4(c). A high correlation was observed within the concentration range of 20–100  $\mu\text{M}$ , yielding a correlation coefficient ( $R^2$ ) of 0.9527. The limit of detection (LOD) was calculated to be 17  $\mu\text{M}$ . These results confirm the feasibility of the proposed sensor with high accuracy for uric acid detection in sweat.

#### D. SERS Sensor for Glucose and pH Detection in Sweat

Glucose molecules possess a small Raman scattering cross-section and lack chemical affinity towards SERS substrates like gold or silver. This leads to the generation of exceedingly weak SERS signals from glucose molecules, easily overshadowed by the strong background noise in the surrounding environment [57]. Consequently, there are limitations in utilizing

non-labeled detection methods for the rapid assessment of glucose levels in sweat. The schematic in Fig. 5(a) outlines the detection principle employed in this study, where the B-OH group of 4-MPBA binds with glucose molecules, forming a cis-diol complex [58] that diminishes the characteristic peak at  $1068\text{ cm}^{-1}$  associated with B-OH. Through modification of AgNPs with 4-MPBA, the B-OH stretching pattern at  $1068\text{ cm}^{-1}$  can be used to quantitatively detect glucose concentration [59]. As depicted in Fig. 5(a), the peak at  $1068\text{ cm}^{-1}$  diminishes as the glucose concentration in sweat increases.

Then, the capability of the SERS sensor for glucose was investigated in the concentration range of 1  $\mu\text{M}$ –1 mM, which covers the range of sweat glucose concentrations in healthy humans as well as diabetic patients, as shown in Fig. 5(b). The quantitative measurement of glucose concentration by comparing the difference between the change in SERS intensity and the initial intensity yielded a calibration curve as shown in Fig. 5(c), which shows good linear correlation in the concentration range of 1  $\mu\text{M}$ –1 mM with a correlation coefficient  $R^2$  of 0.9614. In addition, to validate the specificity of this sensor for glucose detection, we chose the same concentrations of the

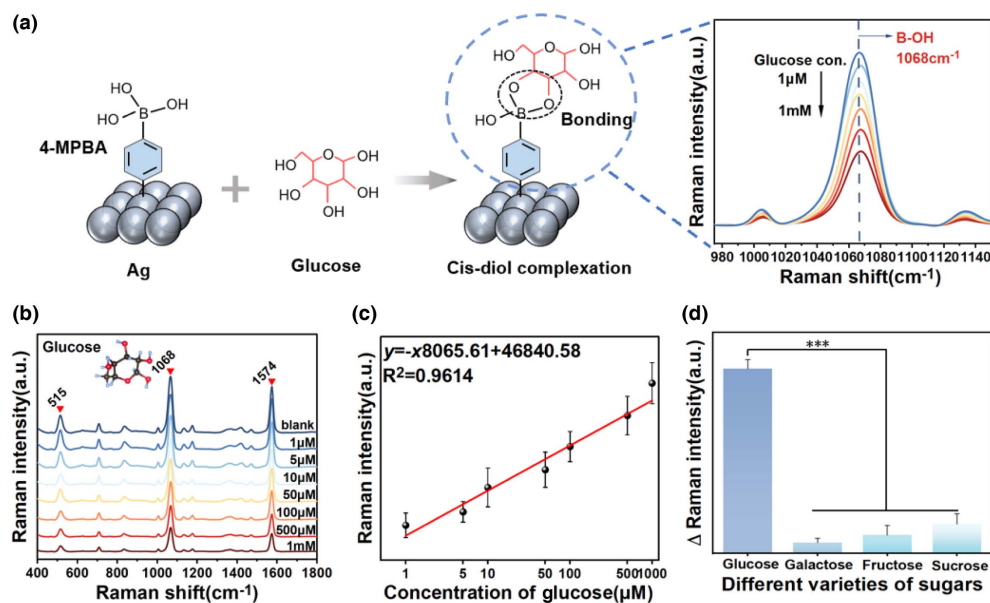


**Fig. 5.** SERS sensor for detecting glucose in sweat. (a) Schematic of the detection principle of glucose. (b) SERS spectra of different concentrations (1–1000  $\mu\text{M}$ ) of glucose in sweat. (c) Linear fitting curve of SERS intensity at 4-MPBA characteristic peak  $1068\text{ cm}^{-1}$ . (d) Selective sensing of glucose by SERS sensor.

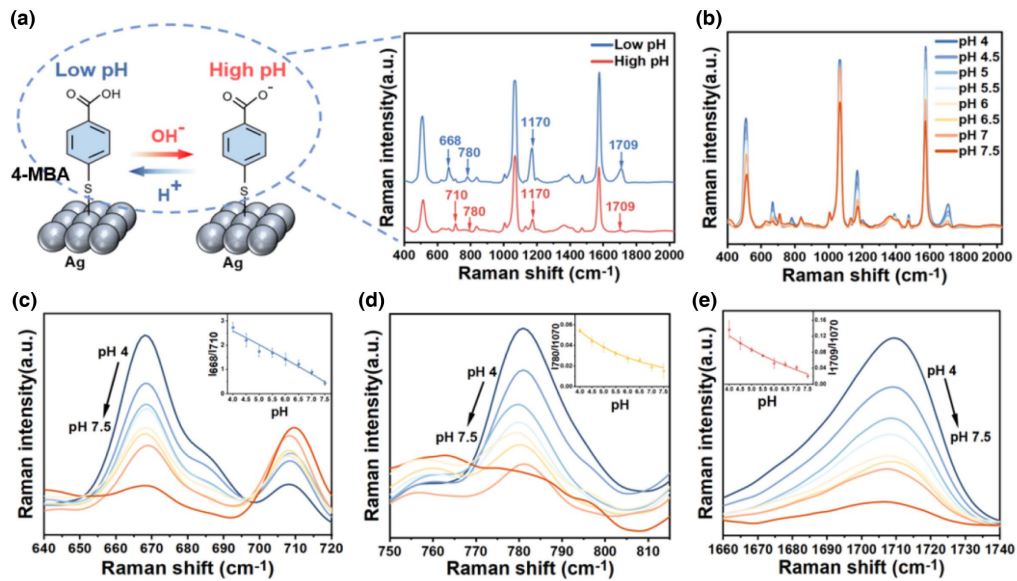


**Fig. 6.** SERS sensor for detecting pH in sweat. (a) Schematic of the detection principle of pH in sweat. (b) SERS spectra of sweat with different pH values. (c) Amplified SERS spectra at 640–720  $\text{cm}^{-1}$ , inset for  $I_{668}/I_{710}$  at different pH. (d) Amplified SERS spectra at 750–820  $\text{cm}^{-1}$ , inset for  $I_{780}/I_{1070}$  at different pH. (e) Amplified SERS spectra at 1660–1740  $\text{cm}^{-1}$ , inset for  $I_{1709}/I_{1070}$  at different pH.

fructose, galactose, sucrose, and glucose for comparison tests as shown in Fig. 5(d), and found that the binding of B-OH groups to glucose showed higher affinity by measuring the change in Raman intensity via the intensity comparison. The above results demonstrate that the sensitive and specific quantitative detection of glucose in sweat can be achieved by the proposed SERS sensor.

Sweat pH serves as a crucial indicator for assessing the acid-base balance in the human body and gauging the skin's health. Consequently, the wearable sweat sensor device under investigation can play a pivotal role in monitoring sweat pH to enhance our understanding of human health. The operational concept of this sweat sensor for pH detection is depicted in Fig. 6(a). The sulfur group (-SH) found in 4-MBA acts as a pH-sensitive probe that can be affixed onto AgNPs via Ag-S bonding. In distinct acidic and alkaline environments, 4-MBA assumes different ionization states, protonating when exposed to acidity and deprotonating in alkaline conditions, consequently resulting in shifts in position and intensity [49,60].

Human sweat typically exhibits pH levels ranging from 4.5 to 7, aligning with the span of our measurements. Changes in SERS characteristic peaks within the 640–720  $\text{cm}^{-1}$ , 750–820  $\text{cm}^{-1}$ , and 1660–1740  $\text{cm}^{-1}$  regions corresponding to pH variations are delineated in Figs. 6(b)–6(e). For instance, Fig. 6(c) illustrates a significant blue shift in characteristic peaks between 668 and 710  $\text{cm}^{-1}$  with a rise in pH from 4 to 7.5. The insets in Figs. 6(c)–6(e) showcase calibration curves of various spectral bands ( $I_{668}/I_{710}$ ,  $I_{780}/I_{1070}$ ,  $I_{1709}/I_{1070}$ ) displaying proportional alterations with pH increments. These findings underscore the device's sensitive and quantitative capacity for sweat pH analysis.

### E. Utility of the Flexible Wearable Chip

Response time is a critical performance metric for wearable sweat sensors, enabling rapid detection of target molecule

concentration changes and real-time physiological feedback for dynamic health monitoring. This study systematically evaluated the sensor's response time, and results showed that the SERS signals tended towards stability after 5 min for uric acid and glucose, and 15 min for pH detection, depicted in Fig. 7.

Next, the performance assessment of the flexible wearable device for sweat collection and SERS analysis was conducted on a human subject. A soft, thin, paper-based microfluidic wearable chip was seamlessly integrated onto the skin surface, as illustrated in Fig. 8(a). The optical depiction of the sensor affixed to the human forearm is presented in Figs. 8(b) and 8(c). The presence of a soft, breathable waterproof encapsulation layer significantly bolsters the device's robustness, mechanical deformation tolerance, and comfort when worn. It adeptly conforms to natural body movements, accommodating skin stretching without causing irritation, thus ensuring stable and non-intrusive SERS analysis in real-life scenarios. This configuration establishes a dependable foundation for prolonged sensor operation in unaltered conditions. The chip is pliable and resistant to deformation. In Fig. 8(d), a snapshot depicts a volunteer wearing the sensor while engaging in a vigorous pull-down exercise, showcasing its applicability for on-site detection of sweat. Additionally, Fig. 8(e) highlights the straightforward portable design, eliminating the need for large-scale Raman instruments. The operational setup solely requires a hand-held portable Raman spectrometer and a laptop computer, facilitating real-time SERS analysis of sweat constituents. In our paper-based nanoplasmonic microfluidic system, as illustrated in Fig. 8(f), simultaneous detection of three critical parameters (uric acid, glucose, and pH value) in sweat is feasible by incorporating distinct function chips at three independent positions within the microfluidic paper's channels. To validate the feasibility of the sensor in detecting a broad concentration range within real sweat, various concentrations of analytes were

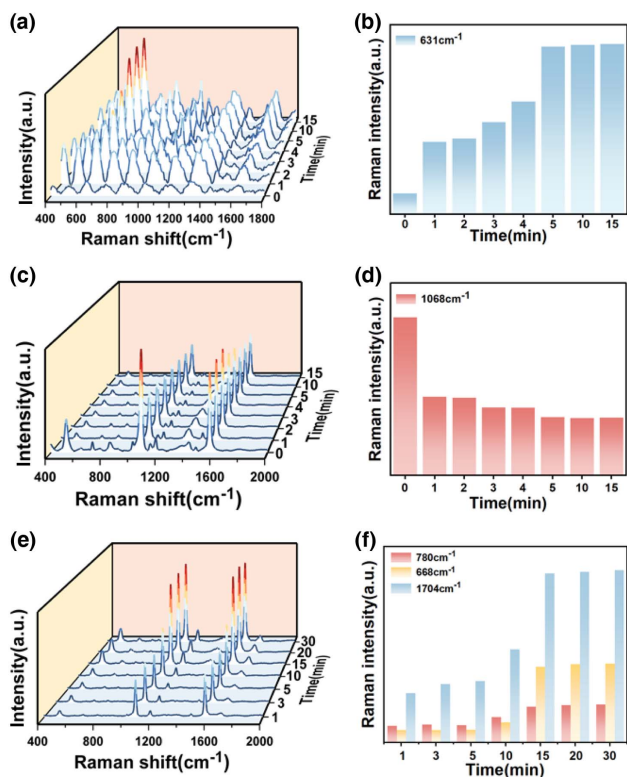


**Fig. 7.** (a) SERS spectra and (b) the Raman intensity of characteristic peak at  $631\text{ cm}^{-1}$  at the response time of 0, 1, 2, 3, 4, 5, 10, 15 min in uric acid test. (c) SERS spectra and (d) the Raman intensity of characteristic peak at  $1068\text{ cm}^{-1}$  at the response time of 0, 1, 2, 3, 4, 5, 10, 15 min in glucose test. (e) SERS spectra and (f) the Raman intensity of characteristic peak at 668, 780, and  $1704\text{ cm}^{-1}$  at the response time of 0, 1, 2, 3, 4, 5, 10, 15 min in pH test.

spiked into real sweat samples. In this study, the recovery rate was determined by comparing the concentration measured using SERS with the spiked concentration [54]. Through SERS detection, the recovery rates of these samples ranged from 95% to 116%, as illustrated in Table 1. This approach was employed to validate the accuracy and anti-interference capability of the SERS method in complex environments, thereby assessing its reliability for practical sample analysis. Furthermore, we compared the concentrations obtained from the calibration curve with the standard concentrations, as depicted in Figs. 8(g)–8(i). The results exhibited a strong correlation and consistent trend, indicating the sensor's feasibility. Additionally, utilizing the methods shown in Figs. 8(d) and 8(e), we collected and analyzed the SERS spectrum of sweat after volunteers wore the sensor for 30 min. As shown in Figs. 8(j)–8(l), the concentration of uric acid, glucose, and pH was determined to be  $22.3\text{ }\mu\text{M}$ ,  $12\text{ }\mu\text{M}$ , and 5.5, respectively, all of which fell within the normal concentration ranges for healthy individuals. This demonstrates the sensor's capability to detect multiple components in real sweat with trace and quantitative accuracy.

Since the sensor is designed for continuous contact with the skin, we used hypoallergenic natural cellulose paper as the main material, and used double-sided medical tape and medical waterproof film as auxiliary materials to reduce the irritation

and injury of the sensor to the human body. In addition, we used a double-sided carbon belt to prevent the damage from laser to the human skin. In order to ensure that the sensor can be used in wearable applications, tests that continuously monitored human skin were performed every 2 h within 12 h, and the results showed that the sensor can be suitable for long-term wear without damage and irritation to human skin.

Currently, the gold standard detection methods for uric acid (serum uricase method), glucose (plasma hexokinase method), and pH (arterial blood gas analysis) all require blood sampling or arterial puncture. While offering high accuracy and clinical diagnostic authority, their invasive nature, operational complexity, and inability for real-time monitoring limit applications in long-term dynamic observation. In contrast, sweat detection technology demonstrates significant advantages: (i) being completely non-invasive, avoiding the discomfort of repeated blood sampling; (ii) enabling synchronous real-time monitoring of multiple indicators including pH, uric acid, and glucose; (iii) easy integration into wearable devices for home or exercise scenarios. Although current sweat detection accuracy remains slightly lower than gold standards, its breakthroughs in continuous monitoring and user experience provide innovative solutions for chronic disease management, health screening, and special populations (e.g., children, athletes), addressing the limitations of traditional methods in dynamic monitoring applications.

#### 4. CONCLUSION

In summary, a wearable paper-based sensing chip based on SERS was developed for *in-situ* detection of sweat. Owing to the soft and stretchable features, the prepared chip can fit perfectly onto the human skin surface where the collection, transmission, and detection of sweat can be simultaneously achieved in this chip. Using this sensor, precise detection and quantification of multiple components in sweat can be performed with the LOD of  $17\text{ }\mu\text{M}$  (uric acid) and  $1\text{ }\mu\text{M}$  (glucose) as well as the range of 4–7.5 for pH values. With the use of a hand-held Raman spectrometer, rapid and real time identification of these valuable parameters of sweat can be achieved, which would offer a POCT manner for personalized health monitoring and medical diagnostics.

Although some satisfactory results have been achieved in this work, there are also some challenges. The current detection approach relying on active perspiration is more suitable for exercise scenarios, presenting certain limitations during resting states or when sweat secretion is low. Therefore, our future research will focus on integrating miniaturized sweat stimulation systems (such as iontophoresis or microneedle patch technologies) with wearable devices. By employing mild physical or chemical stimuli to induce adequate sweat production across various physiological states, we aim to extend the sensor's applicability to resting conditions and low-sweat scenarios. This development will enable the device to not only monitor exercise status but also facilitate continuous biomarker tracking during rest, sleep, and diverse clinical settings, thereby simultaneously meeting the demands of both athletic performance monitoring and general health surveillance. In addition, although the read-out devices of this work are portable Raman instruments and

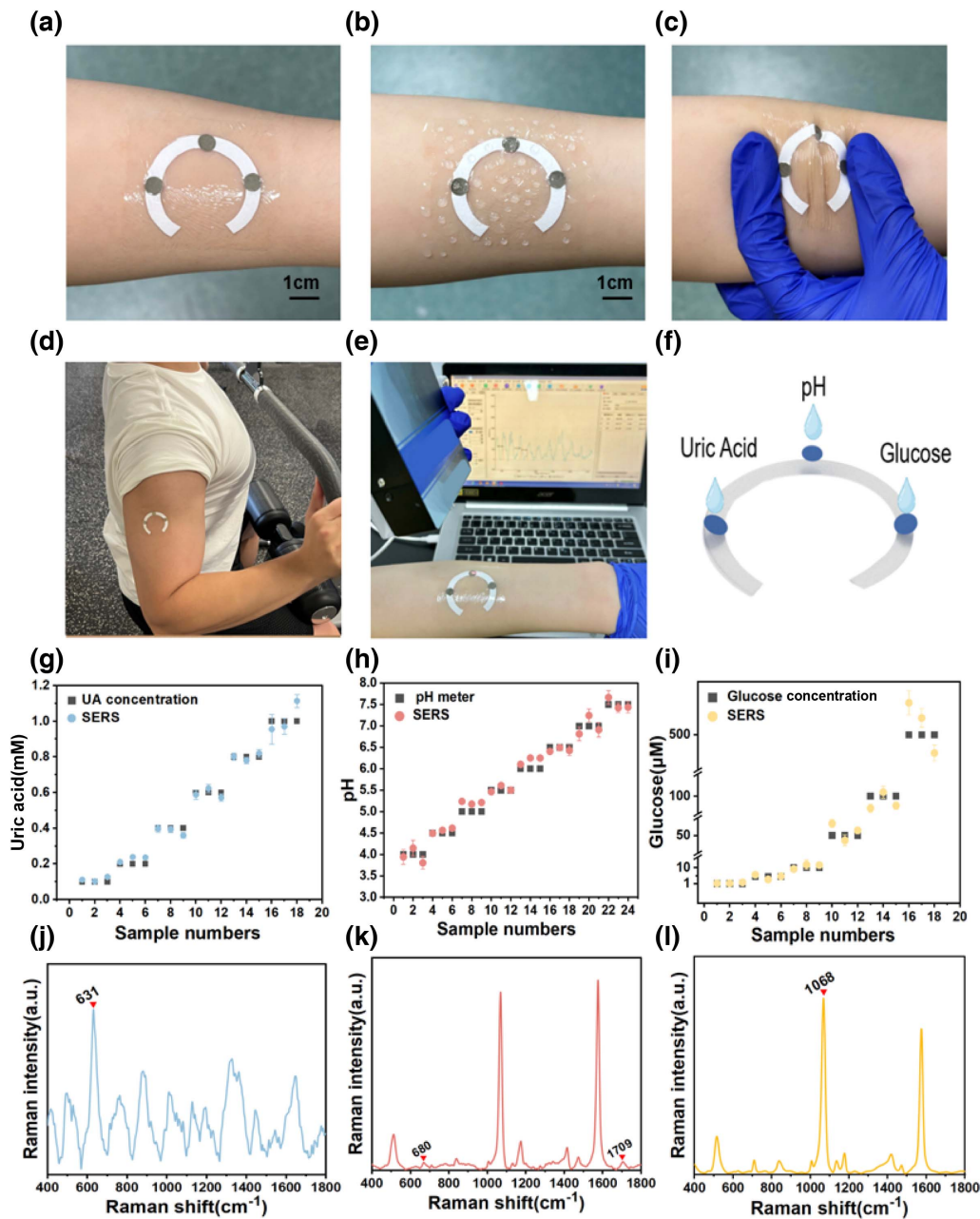


**Fig. 8.** Utility of the flexible wearable chip. (a) Flexible wearable chip fit to the surface of human skin. (b) Waterproof performance test of the flexible wearable chip. (c) Tensile deformation performance test of the flexible wearable chip. (d) Photograph of a volunteer wearing the SERS chip during continuous exercise. (e) *In-situ* SERS analysis using a hand-held Raman spectrometer and a laptop computer. (f) Schematic diagram that allows for simultaneous labeled and unlabeled detection. (g) Comparison between uric acid concentrations determined by the SERS method and standard uric acid concentrations. (h) Comparison of pH calculated by SERS method measurement with commercial pH meter results. (i) Comparison between glucose concentrations determined by the SERS method and standard glucose concentrations. (j) SERS spectrum of real sweat collected from volunteers by uric acid sensor. (k) SERS spectrum of real sweat collected from volunteers by pH sensor. (l) SERS spectrum of real sweat collected from volunteers by glucose sensor.

laptop computers, which have considerable portability, the use of smart phones as readout devices is still an effective means to make wearable devices more portable. The data of the wearable sensor is transmitted to the smartphone via Bluetooth, which is also the direction of our future research, to create a more integrated system enabling better human-device interaction experience and more flexible scenarios.

Although our current detection limits for uric acid ( $17 \mu\text{M}$ ) and glucose ( $1 \mu\text{M}$ ) and pH detection range (4–7.5) can meet some application requirements (such as post-exercise sweat monitoring), and the detection limits are significantly better than those of colorimetric methods ( $20.7 \mu\text{M}$  [31],  $10 \mu\text{M}$  [45]), there is still room for improvement compared with some electrochemical methods ( $0.467 \mu\text{M}$  [4]). However, it should

**Table 1. Determination of Uric Acid, pH, and Glucose in Sweat Samples Using the Wearable Nanoplasmonic Paper-Based Sensor ( $n = 3$ )**

Sample	Spiked Target Concentration	SERS		
		Detected Concentration	Recovery (%)	RSD (%)
Uric acid				
1	0.2 mM	0.23 mM	115	5.80
2	0.4 mM	0.38 mM	95	4.87
3	0.8 mM	0.81 mM	101.2	1.67
pH				
1	4.5	4.56	101.3	1.20
2	5.5	5.53	100.5	1.18
3	6.5	6.44	99.1	0.52
Glucose				
1	1 $\mu$ M	1.16 $\mu$ M	116	3.52
2	100 $\mu$ M	96.73 $\mu$ M	96.7	4.20
3	1000 $\mu$ M	1056.67 $\mu$ M	105.7	2.94

be noted that our SERS sensors have unique advantages: (i) label-free detection capability; (ii) multi-component synchronous analysis (capable of simultaneously detecting pH, uric acid, and glucose); (iii) simple manufacturing process, and low cost (unit price <5 RMB), supporting replacement as needed. In the future, our research will be dedicated to further reducing the detection limit, which can be achieved through the following strategies: (i) developing core-shell structured SERS substrates; (ii) integrating the microfluidic pre-concentration module; (iii) combining machine learning algorithms to eliminate background interference.

Artificial intelligence and machine learning can significantly enhance the performance of SERS-based sweat analysis [61–63]. In our future research, we will focus on integrating deep learning algorithms with our existing SERS sensors to achieve intelligent spectral feature extraction, thereby markedly improving the detection capability for trace biomarkers. Through machine-learning-driven data preprocessing to optimize the signal-to-noise ratio in complex matrices, combined with the development of large-sample-trained intelligent diagnostic models for accurate multiplex detection quantification, we aim to comprehensively improve the sensor's sensitivity and specificity, ultimately facilitating practical clinical applications of wearable sensing devices.

**Funding.** National Natural Science Foundation of China (12374405); Provincial Science Foundation for Distinguished Young Scholars of Fujian (2024J010024); Fuzhou Science and Technology Major Project (2023-ZD-004); Natural Science Foundation of Fujian Province (2023J011267); Joint Funds for the Innovation of Science and Technology, Fujian (2021Y9196); Major Research Projects for Young and Middle-Aged Researchers of Fujian Provincial Health Commission (2021ZQNZD010).

**Disclosures.** The authors declare no conflicts of interest.

**Data Availability.** Data underlying the results presented in this paper are available from the corresponding author upon reasonable request.

## REFERENCES

- X. Peng, K. Dong, C. Ye, *et al.*, "A breathable, biodegradable, antibacterial, and self-powered electronic skin based on all-nanofiber triboelectric nanogenerators," *Sci. Adv.* **6**, eaba9624 (2020).
- G. Liu, Z. Mu, J. Guo, *et al.*, "Surface-enhanced Raman scattering as a potential strategy for wearable flexible sensing and point-of-care testing non-invasive medical diagnosis," *Front. Chem.* **10**, 1060322 (2022).
- H. Q. Liu, Y. N. He, and K. Z. Cao, "Flexible surface-enhanced Raman scattering substrates: a review on constructions, applications, and challenges," *Adv. Mater. Interfaces* **8**, 2100982 (2021).
- Y. Li, Y. Guo, H. Chen, *et al.*, "Flexible wearable plasmonic paper-based microfluidics with expandable channel and adjustable flow rate for portable surface-enhanced Raman scattering sweat sensing," *ACS Photonics* **11**, 613–625 (2024).
- T. Laochai, C. Moonla, J. M. Moon, *et al.*, "Touch-based potentiometric sensors for simultaneous detection of urea and ammonium from fingertip sweat," *Sens. Actuators B Chem.* **413**, 135898 (2024).
- B. Tasangtong, K. Sirichan, C. Hasoon, *et al.*, "Fabrication of biocompatible and biodegradable cloth-based sweat sensors using polylactic acid (PLA) via stencil transparent film-printing," *Sens. Actuators B Chem.* **408**, 135513 (2024).
- Y. Shi, L. Wang, Y. Hu, *et al.*, "Contact lens sensor for ocular inflammation monitoring," *Biosens. Bioelectron.* **249**, 116003 (2024).
- K. V. Jarnda, D. Wang, A. Ul Qurrat, *et al.*, "Recent advances in electrochemical non-enzymatic glucose sensor for the detection of glucose in tears and saliva: a review," *Sens. Actuators A Phys.* **363**, 114778 (2023).
- X. Ma, L. Deng, Z. Zou, *et al.*, "Novel portable photoelectrochemical sensor based on CdS/Au/TiO<sub>2</sub> nanotube arrays for sensitive, non-invasive, and instantaneous uric acid detection in saliva," *Talanta* **271**, 125646 (2024).
- V. T. N. Linh, H. Kim, M.-Y. Lee, *et al.*, "3D plasmonic hexaplex paper sensor for label-free human saliva sensing and machine learning-assisted early-stage lung cancer screening," *Biosens. Bioelectron.* **244**, 115779 (2024).
- T.-Q. Ma, Q.-Y. He, X.-Y. Li, *et al.*, "Wearable microneedle sensor with replaceable sensor base for multi-purpose detecting in skin interstitial fluid," *Microchem. J.* **203**, 110933 (2024).
- H. Piao, Y.-H. Choi, J. Kim, *et al.*, "Impedance-based polymer microneedle patch sensor for continuous interstitial fluid glucose monitoring," *Biosens. Bioelectron.* **247**, 115932 (2024).
- Y. Li, H. Chen, Y. Guo, *et al.*, "Lamellar hafnium ditelluride as an ultra-sensitive surface-enhanced Raman scattering platform for label-free detection of uric acid," *Photonics Res.* **9**, 1039–1047 (2021).
- C. Wang, Y. Zhang, Y. Liu, *et al.*, "A wearable flexible electrochemical biosensor with CuNi-MOF@rGO modification for simultaneous detection of uric acid and dopamine in sweat," *Anal. Chim. Acta* **1299**, 342441 (2024).
- Z. Xu, J. Song, B. Liu, *et al.*, "A conducting polymer PEDOT:PSS hydrogel based wearable sensor for accurate uric acid detection in human sweat," *Sens. Actuators B Chem.* **348**, 130674 (2021).
- D. Jiang, Y. Zhu, Z. Sun, *et al.*, "A silver nanowires@Prussian blue composite aerogel-based wearable sensor for noninvasive and dynamic monitoring of sweat uric acid," *Chem. Eng. J.* **486**, 150220 (2024).
- A. Xu, M. Xu, F. Luo, *et al.*, "Realizing high-performance glucose sensing in sweat: synergistic use of nickel oxide nanosheets as photoelectrodes and the masking effect of Mo-POM for photoelectrochemical detection," *Sens. Actuators B Chem.* **403**, 135135 (2024).
- V. Kansay, V. Dutt Sharma, V. Srivastava, *et al.*, "Wearable, disposable and non-enzymatic fluorescence nanosensor for monitoring sweat glucose through smartphone," *Microchem. J.* **201**, 110624 (2024).
- J. Moyer, D. Wilson, I. Finkelshtein, *et al.*, "Correlation between sweat glucose and blood glucose in subjects with diabetes," *Diabetes Technol. Ther.* **14**, 398–402 (2012).
- X. Cui, Y. Bao, T. Han, *et al.*, "A wearable electrochemical sensor based on  $\beta$ -CD functionalized graphene for pH and potassium ion analysis in sweat," *Talanta* **245**, 123481 (2022).

21. Q. Xie, R. Li, and Z. Li, "Designing of multifunctional graphene quantum dot-polyvinyl alcohol-polyglycerol luminescent film for fluorescence detection of pH in sweat," *Anal. Chim. Acta* **1292**, 342224 (2024).
22. P. Escobedo, C. E. Ramos-Lorente, A. Martínez-Olmos, *et al.*, "Wireless wearable wristband for continuous sweat pH monitoring," *Sens. Actuators B Chem.* **327**, 128948 (2021).
23. W. Ji, J. Zhu, W. Wu, *et al.*, "Wearable sweat biosensors refresh personalized health/medical diagnostics," *Research* **2021**, 9757126 (2021).
24. F. Gao, C. Liu, L. Zhang, *et al.*, "Wearable and flexible electrochemical sensors for sweat analysis: a review," *Microsyst. Nanoeng.* **9**, 1 (2023).
25. Z. Xu, X. Qiao, R. Tao, *et al.*, "A wearable sensor based on multifunctional conductive hydrogel for simultaneous accurate pH and tyrosine monitoring in sweat," *Biosens. Bioelectron.* **234**, 115360 (2023).
26. N. Promphet, C. Thanawattano, C. Buekban, *et al.*, "Smartphone based wearable sweat glucose sensing device correlated with machine learning for real-time diabetes screening," *Anal. Chim. Acta* **1312**, 342761 (2024).
27. X. Mei, J. Yang, X. Yu, *et al.*, "Wearable molecularly imprinted electrochemical sensor with integrated nanofiber-based microfluidic chip for in situ monitoring of cortisol in sweat," *Sens. Actuators B Chem.* **381**, 133451 (2023).
28. Y. Yin, Z. Tan, W. Zhu, *et al.*, "A wearable microfluidic system for efficient sweat collection and real-time detection," *Talanta* **274**, 125967 (2024).
29. J. Kim, S. Oh, D. S. Yang, *et al.*, "A skin-interfaced, miniaturized platform for triggered induction, capture and colorimetric multicomponent analysis of microliter volumes of sweat," *Biosens. Bioelectron.* **253**, 116166 (2024).
30. P. Xi, X. He, C. Fan, *et al.*, "Smart Janus fabrics for one-way sweat sampling and skin-friendly colorimetric detection," *Talanta* **259**, 124507 (2023).
31. B. Fan, Y. Wu, H. Guo, *et al.*, "Self-assembly of cascade nanoenzyme glucose oxidase encapsulated in copper benzenedicarboxylate for wearable sweat-glucose colorimetric sensors with smartphone read-out," *Anal. Chim. Acta* **1316**, 342852 (2024).
32. W. Wang, Y. Chen, C. Xiao, *et al.*, "Flexible SERS wearable sensor based on nanocomposite hydrogel for detection of metabolites and pH in sweat," *Chem. Eng. J.* **474**, 145953 (2023).
33. Y. Guo, Y. Liu, C. Luo, *et al.*, "Instantaneous preparation of gold-carbon dot nanocomposites for on-site SERS identification of pathogens in diverse interfaces," *Photonics Res.* **12**, 1303–1312 (2024).
34. J. Langer, D. J. de Aberasturi, J. Aizpurua, *et al.*, "Present and future of surface-enhanced Raman scattering," *ACS Nano* **14**, 28–117 (2019).
35. S. Lee, H. Dang, J.-I. Moon, *et al.*, "SERS-based microdevices for use as *in vitro* diagnostic biosensors," *Chem. Soc. Rev.* **53**, 5394–5427 (2024).
36. H. Ma, S.-Q. Pan, W.-L. Wang, *et al.*, "Surface-enhanced Raman spectroscopy: current understanding, challenges, and opportunities," *ACS Nano* **18**, 14000–14019 (2024).
37. C. Zong, M. Xu, L. J. Xu, *et al.*, "Surface-enhanced Raman spectroscopy for bioanalysis: reliability and challenges," *Chem. Rev.* **118**, 4946–4980 (2018).
38. D. Cialla-May, A. Bonifacio, T. Bocklitz, *et al.*, "Biomedical SERS—the current state and future trends," *Chem. Soc. Rev.* **53**, 8957–8979 (2024).
39. D. Lu, R. Cai, Y. Liao, *et al.*, "Two-dimensional glass/p-ATP/Ag NPs as multifunctional SERS substrates for label-free quantification of uric acid in sweat," *Spectrochim. Acta A* **296**, 122631 (2023).
40. L. Fan, Z. Wang, Y. Zhang, *et al.*, "Molecularly imprinted monolithic column-based SERS sensor for selective detection of cortisol in dog saliva," *Talanta* **249**, 123609 (2022).
41. S. Xiong, C. Wang, T. Wang, *et al.*, "Label-free detection of sweat biomarkers using AuNRAs-based SERS-digital microfluidic sensor," *Chem. Eng. J.* **510**, 161849 (2025).
42. M. S. S. Bharati and V. R. Soma, "Flexible SERS substrates for hazardous materials detection: recent advances," *Opto-Electron. Adv.* **4**, 210048 (2021).
43. B. Chen, J. Gao, H. Sun, *et al.*, "Wearable SERS devices in health management: challenges and prospects," *Spectrochim. Acta A* **334**, 125957 (2025).
44. M. Chung, W. H. Skinner, C. Robert, *et al.*, "Fabrication of a wearable flexible sweat pH sensor based on SERS-active Au/TPU electrospun nanofibers," *ACS Appl. Mater. Interfaces* **13**, 51504–51518 (2021).
45. Q. Niu, R. Yuan, H. Zhan, *et al.*, "Janus membrane-based wearable dual-channel SERS sensor for sweat collection and monitoring of lactic acid and pH levels," *Anal. Chem.* **97**, 6083–6091 (2025).
46. Z. Chen, W. Wang, H. Tian, *et al.*, "Wearable intelligent sweat platform for SERS-AI diagnosis of gout," *Lab Chip* **24**, 1996–2004 (2024).
47. X. Zhang, X. Wang, M. Ning, *et al.*, "Fast synthesis of Au nanoparticles on metal–phenolic network for sweat SERS analysis," *Nanomaterials* **12**, 2977 (2022).
48. M. Umeha, G. Heng, N. Myeong, *et al.*, "Wearable plasmonic paper-based microfluidics for continuous sweat analysis," *Sci. Adv.* **8**, eabn1736 (2022).
49. X. He, C. Fan, Y. Luo, *et al.*, "Flexible microfluidic nanoplasmonic sensors for refreshable and portable recognition of sweat biochemical fingerprint," *npj Flexible Electron.* **6**, 60 (2022).
50. N. Leopold and B. Lendl, "A new method for fast preparation of highly surface-enhanced Raman scattering (SERS) active silver colloids at room temperature by reduction of silver nitrate with hydroxylamine hydrochloride," *J. Phys. Chem. B* **107**, 5723–5727 (2003).
51. T. N. Q. Trang, N. T. G. Bao, L. Q. Vinh, *et al.*, "Centrifuge tube-based SERS sensor on heterogenous dimers of plasmonic coupling as a microreactor for ultrasensitive SERS sensing pesticide residues in environmental water," *Sens. Actuators A Phys.* **369**, 115173 (2024).
52. H. Xin, W. J. Sim, B. Namgung, *et al.*, "Quantum biological tunnel junction for electron transfer imaging in live cells," *Nat. Commun.* **10**, 3245 (2019).
53. B. X. Hu, H. B. Pu, and D.-W. Sun, "Multifunctional cellulose based substrates for SERS smart sensing: principles, applications and emerging trends for food safety detection," *Trends Food Sci. Technol.* **110**, 304–320 (2021).
54. B. Sharma, R. R. Frontiera, A.-I. Henry, *et al.*, "SERS: materials, applications, and the future," *Mater. Today* **15**, 16–25 (2012).
55. Z. Wang, L. Zhang, L. Sun, *et al.*, "Self-assembly flexible SERS imprinted membrane based on Ag nanocubes for selective detection of microcystin-LR," *Microchim. Acta* **191**, 19 (2023).
56. Y. Yang, Y. Song, X. Bo, *et al.*, "A laser-engraved wearable sensor for sensitive detection of uric acid and tyrosine in sweat," *Nat. Biotechnol.* **38**, 217–224 (2019).
57. D. Yang, S. Afroosheh, J. O. Lee, *et al.*, "Glucose sensing using surface-enhanced Raman-mode constraining," *Anal. Chem.* **90**, 14269–14278 (2018).
58. D. Wang, G. C. Xu, X. S. Zhang, *et al.*, "Dual-functional ultrathin wearable 3D particle-in-cavity SF-AAO-Au SERS sensors for effective sweat glucose and lab-on-glove pesticide detection," *Sens. Actuators B Chem.* **359**, 131512 (2022).
59. H. Torul, H. Çiftçi, D. Çetin, *et al.*, "Paper membrane-based SERS platform for the determination of glucose in blood samples," *Anal. Bioanal. Chem.* **407**, 8243–8251 (2015).
60. A. Quinn, Y.-H. You, and M. J. McShane, "Hydrogel microdomain encapsulation of stable functionalized silver nanoparticles for SERS pH and urea sensing," *Sensors* **19**, 3521 (2019).
61. Z. Chen, Y. Liu, W. Yu, *et al.*, "Machine learning-driven wearable sweat sensors with AgNW/MXene for non-invasive SERS-based cardiovascular disease detection," *ACS Appl. Nano Mater.* **8**, 5602–5610 (2025).
62. S. Laing, S. Sloan-Dennison, K. Faulds, *et al.*, "Surface enhanced Raman scattering for biomolecular sensing in human healthcare monitoring," *ACS Nano* **19**, 8381–8400 (2025).
63. X. Jin, C. Liu, T. Xu, *et al.*, "Artificial intelligence biosensors: challenges and prospects," *Biosens. Bioelectron.* **165**, 112412 (2020).